© 2018. Published by The Company of Biologists Ltd | Journal of Experimental Biology (2018) 221, jeb174540. doi:10.1242/jeb.174540

RESEARCH ARTICLE

Resistance to DNA damage and enhanced DNA repair capacity in the hypoxia-tolerant blind mole rat *Spalax carmeli*

Vered Domankevich, Hossam Eddini, Amani Odeh and Imad Shams*

ABSTRACT

Blind mole rats of the genus *Spalax* are the only mammalian species to date for which spontaneous cancer has never been reported and resistance to carcinogen-induced cancers has been demonstrated. However, the underlying mechanisms are still poorly understood. The fact that *Spalax* spp. are also hypoxia-tolerant and long-lived species implies the presence of molecular adaptations to prevent genomic instability, which underlies both cancer and aging. We previously demonstrated the upregulation of transcripts related to DNA replication and repair pathways in *Spalax*. Yet, to date, no direct experimental evidence for improved genomic maintenance has been demonstrated for this genus. Here, we show that compared with skin fibroblasts of the above-ground rat, *Spalax carmeli* skin fibroblasts in culture resist several types of genotoxic insult, accumulate fewer genotoxic lesions and exhibit an enhanced DNA repair capacity. Our results strongly support that this species has evolved efficient mechanisms to maintain DNA integrity as an adaptation to the stressful conditions in the subterranean habitat.

KEY WORDS: DNA repair, Hypoxia, Longevity, Cell cycle, Genotoxic stress, Cancer

INTRODUCTION

The blind mole rats, *Spalax*, endure extreme and abrupt fluctuations in O_2 and CO_2 levels and survive very low oxygen content (down to 3% O_2) (Shams et al., 2005; Avivi et al., 1999). Under hypoxic conditions, deoxynucleotide triphosphates (dNTPs) are depleted and DNA repair pathways are repressed. The subsequent re-oxygenation leads to replication restart in the presence of oxidative DNA damage even though DNA repair mechanisms have not yet been recovered (Pires et al., 2010; Klein and Glazer, 2010). In other mammalian species, cycles of acute oxygen fluctuations act as a driving force of genomic instability (Klein and Glazer, 2010). However, *Spalax* spp. are long-lived (Tacutu et al., 2013) and, to date, no single case of spontaneous cancer has been reported for these species, during decades of research.

In a previous study, we attempted to induce cellular transformation in *Spalax*, *in vivo*, using two types of carcinogens (Manov et al., 2013): (1) DMBA/TPA – a skin carcinogenesis protocol was used to treat eight *Spalax* and six mice individuals; and (2) 3MCA – a local fibrosarcoma induction protocol was used to treat 12 *Spalax*, six mouse and six rat individuals. Whereas all mice and rats developed the expected tumors within 2–6 months, no tumors were observed among *Spalax* individuals treated with DMBA/TPA. 3MCA treatmentinduced benign fibroblastic proliferation in only two *Spalax* individuals, and malignancies in another two individuals within 18 months (Manov et al., 2013) and 30 months (I.S., unpublished data).

The naked mole rat (*Heterocephalus glaber*) is another subterranean rodent that is phylogenetically distant from *Spalax* (estimated divergence time from *Spalax* is 73 million years ago, whereas that of the rat and mouse is 45 million years ago) (Hedges et al., 2006). Remarkably, in addition to their hypoxia tolerance, three very exceptional traits have evolved in these species: (1) an ability to secrete anti-cancer substances in conditioned media (Manov et al., 2013); (2) a very low frequency of spontaneous cancers (Manov et al., 2013; Delaney et al., 2016; Buffenstein, 2005); and (3) an increased lifespan, relative to body mass (Tacutu et al., 2013; Gorbunova et al., 2014). This suggests that inhabiting hypoxic environments may require the ability to overcome a greater risk for cancer and aging, possibly because of threats placed by the conditions in these environments on the integrity of genome.

In previous studies, *Spalax* and *H. glaber* genomes have been sequenced, genomic and transcriptomic data have been analyzed (Fang et al., 2014; Kim et al., 2011; Macrae et al., 2015b; Malik et al., 2011; Vinogradov, 2015), cross-species comparative studies have been carried out (Gorbunova et al., 2014; Macrae et al., 2015a,b; Malik et al., 2016; Ma et al., 2016) and reviewed (Gorbunova et al., 2014; Ma and Gladyshev, 2017; Lewis et al., 2016), and several specific candidate mechanisms have been investigated (Tian et al., 2013; Gorbunova et al., 2012; Nasser et al., 2009; Ellis et al., 2016; Zhao et al., 2014; Salmon et al., 2008; Lewis et al., 2012, 2015; Shams et al., 2013; Domankevich et al., 2016; Avivi et al., 2007; Miyawaki et al., 2016). These studies showed that several factors may act in concert to reduce cancer and aging in these species, and that these two subterranean taxa have evolved distinct mechanisms, which allow each to survive its unique physical and social environments. Nevertheless, it was clearly identified that these hypoxia-tolerant mammals express higher transcript levels of DNA repair factors (Macrae et al., 2015a; Malik et al., 2016; Shams et al., 2013), strengthening the assumption that these mammals have evolved common adaptations to hypoxia that include efficient DNA repair mechanisms. Yet, to date, no direct experimental evidence has been provided for this assumption.

Here, we investigated the response to genotoxic stress and the DNA repair capacity in *Spalax carmeli* (Nevo et al., 2001), compared with the above-ground murine *Rattus norvegicus* (hereafter, rat). Our main hypothesis was that *S. carmeli* survives better genotoxic stress and repairs DNA more efficiently. The results presented here provide the first evidence for genotoxic stress resistance and enhanced repair capacity in this species.

MATERIALS AND METHODS

Animals

All experimental protocols were approved by the Institutional Ethics Committee (Institutional Review Board to Evaluate Animal Subject

The Institute of Evolution and Department of Evolutionary and Environmental Biology, University of Haifa, Haifa 3498838, Israel.

*Author for correspondence (imad.shams@univ.haifa.ac.il)

V.D., 0000-0003-3579-4616; I.S., 0000-0001-6496-2928

Received 22 November 2017; Accepted 2 March 2018

Journal of Experimental Biology (2018) 221, jeb174540. doi:10.1242/jeb.174540

Research of the University of Haifa, permit 316/14) and all methods were carried out in accordance with the relevant guidelines and regulations. Primary dermal fibroblasts were isolated from newborn animals (unknown sex). Pregnant rat individuals were purchased from ENVIGO, Israel, and kept in the animal facility of the University of Haifa until birth. *Spalax carmeli* cannot be bred in captivity and thus newborn individuals were captured during the winter season in the field (see Table S1) from three different geographical areas of the *S. carmeli* population in Israel at three different years. Animals were scarified for skin fibroblast isolation by an inhalation anesthesia agent (isoflurane) overdose.

Cell culture

Primary *S. carmeli* and rat skin fibroblasts were isolated as described previously (Glaysher and Cree, 2011) and grown in DMEM-F12 medium (Biological Industries, Beit Haemeq, Israel), supplemented with 15% fetal bovine serum (FBS), L-glutamine, penicillin and streptomycin (Biological Industries). Cells were incubated in a humidified atmosphere of 5% CO_2 and 95% ambient air (unless stated otherwise) at 37°C.

Stress treatments

Cells in log-phase growth, at their third passage, were seeded in multi-well plates (according to experimental settings). When cells reached 80% confluence, the stress treatment was introduced as follows. For the oxidative stress treatment, the medium was replaced with a serum-free medium containing hydrogen peroxide solution (216763, Sigma-Aldrich, St Louis, MO, USA) in concentrations of 50, 100 and 300 µmol l^{-1} for 30 min on ice, unless stated otherwise. After the incubation period, the medium was aspirated, wells were washed with PBS and a complete medium was added to the wells. For topoisomerase inhibition, the cell medium was replaced with medium containing etoposide (Sigma-Aldrich, E1383) dissolved in DMSO in concentrations of 50, 100, 150 and 200 µmol l^{-1}, unless stated otherwise. Following a 24 h incubation period at 37°C, wells were washed with PBS and a complete medium was added. For UV-C radiation, the lid was removed and the plate was placed in the center of a UVC-500 crosslinker (Hoefer, San Francisco, CA, USA) in the presence of medium. Then, a 2000, 4000, 6000 or 8000 J m^{-2} UV-C radiation dose (254 nm wavelength) was applied. In the case of multiple plates, the UV-C radiation treatment was given in aliquots to allow plate rotation in order to ensure equal distribution of the UV rays across the plates. For the hypoxia treatment, cells were placed in a hypoxia incubator under 0.5% O_2 for 10 h (unless stated otherwise).

Cell cycle distribution and apoptosis assay

Cells were seeded in six-well plates and then subjected to H_2O_2 treatment of 150 µmol l^{-1} for 20 min on ice (in two of the three experiments, duplicates were used for each treatment). Following treatment, cells were washed in PBS and medium was replaced (excluding the 0 h time point) with complete medium. Cells were then incubated for an additional 0–4, 24 and 48 h. Following the incubation period, cell cycle distribution was measured by flow cytometry of propidium iodide (PI)-stained nuclei. Cells were harvested by trypsin into polypropylene tubes, washed three times in PBS and re-suspended in hypotonic PI solution (PI 50 µg ml^{-1} in 0.1% sodium citrate plus 0.1% Triton X-100, Sigma-Aldrich). The PI fluorescence of individual nuclei was measured by a FACSaria flow cytometer (Becton Dickinson, Franklin Lakes, NJ, USA). The incidence of apoptotic cells was expressed as the percentage of hypodiploid nuclei.

Viability assay

To assess cell viability, PrestoBlue© reagent was used as follows. Cells were seeded in 96-well plates in four to five replicates. Following treatment, the cell medium was aspirated and Phenol-Red-free DMEM medium containing 10% PrestoBlue© was added to each well. After an additional incubation period (~2 h), each plate was processed throughout the plate reader at wavelengths of 570 and 600 nm. Viability values were calculated as follows (according to the viability reagent manufacturer's instructions): (OD_{570}–blank)−(OD_{600}–blank), where OD is optical density.

Single-cell electrophoresis assay (comet assay)

The alkaline comet assay was employed using the CometAssay Kit, according to the manufacturer's instructions (Trevigen, Gaithersburg, MD, USA). Following stress treatment, cells were harvested by trypsin and cryopreserved in aliquots at −80°C. On the day of the assay, cells were thawed in 37°C, washed in PBS and centrifuged (200 ***g***, 4°C) for 5 min. The cell pellet was then suspended in PBS (calcium- and magnesium-free), added to 37°C low-melting agarose (LMA) and spread onto the slide's wells in duplicate. LMA was allowed to solidify for 10–15 min at 4°C, after which the slide was immersed in lysis solution for 30–60 min and in freshly prepared alkaline unwinding solution for 20 min at room temperature in the dark. For electrophoresis, a cooled electrophoresis tank containing alkaline electrophoresis solution was set to 21 V (constant) and the current was applied for 30 min. Following electrophoresis, slides were washed twice in dH_2O and once in cold 80% ethanol. Slides were then stained with 1:10,000 SYBR® Green I (s7563, Thermo Fisher Scientific, Waltham, MA, USA) staining solution (diluted 1:10,000 in TE buffer, pH 7.5) and then visualized in a Leica DMR fluorescent microscope (at 20× enlargement, Leica, Wetzlar, Germany). Images were taken with a Leica DFC300FX camera and at least 90 comets were scored per sample. Quantification of DNA damage was performed using CaspLab software (Supplier, Town, State, Country).

Immunofluorescence for γ-H2AX foci

Cells were seeded in a six-well plate on coverslips at ~40,000 cells per well. Following a recovery period of 24–48 h, the stress treatment was applied. Cells were then washed twice in PBS and fixated in cold methanol for 2 min. Following fixation, cells were washed three times in a washing buffer (1% Tween, 0.5% Triton, 0.1% BSA in PBS) and blocked in a blocking buffer (1% BSA in washing buffer) for 1 h at room temperature and then incubated with anti-γ-H2AX primary antibody (ab2893, Abcam, Cambridge, UK; diluted 1:700 in blocking buffer) overnight at 4°C, and washed three times in washing buffer. Cells were then incubated with the secondary antibody (711-225-152, Jackson ImmunoResearch Laboratories, West Grove, PA, USA), diluted (1:100–200 in blocking buffer) in the dark for 1 h at room temperature and washed three times in a washing buffer. Cell nuclei were stained by incubation with 300 nmol l^{-1} DAPI solution (Sigma-Aldrich, D9542) for 5 min at room temperature. Following washing two times with a washing buffer and one time with PBS (calcium and magnesium free), coverslips were mounted with ~20 µl of anti-fade mounting medium (9 ml glycerol, 1 ml 1 mol l^{-1} Tris, pH 8, 0.05 g *n*-propyl gallate) on clean, dry slides with cells facing down. Cell nuclei were visualized under a fluorescent microscope (Leica DMi8, equipped with incubator and Leica DFC365FX camera). For 2D imaging of DSBs induced by etoposide, 63× magnification was used. For imaging of DSBs induced by H_2O_2, 100× magnification was used, and 3D images were obtained using tomography. These

images were later used for projection of the nuclei to 2D images. The 2D images were used for quantification of the γ-H2AX foci using FociCounter software (minimum nuclei number=55).

Host cell reactivation assay

peGFPN1 plasmids were diluted to 50 µg ml^{-1} and treated as follows. (1) Plasmid (1 ml) was pipetted into a 100 mm tissue culture dish, which was then placed in a UVC 500 crosslinker (Hoefer). Following a dose of 420, 620 or 1020 J m^{-2}, 100 µl of the treated diluted plasmids was collected into microtubes. (2) For H_2O_2 treatment, 20 µl hydrogen peroxide (Sigma-Aldrich, 216763) was dissolved in 80 µl of 50 µg ml^{-1} plasmid for 1 h at room temperature. Plasmids were then precipitated in ethanol and resolved in 15 µl H_2O. Finally, a NanoDrop© spectrophotometer was used to determine the plasmid concentration, and plasmids were stored at −20°C until transfection.

Spalax carmeli and rat skin fibroblasts were seeded in 48-well plates in duplicate and transfected according to the 'hard-to-transfect' PolyJet© protocol, with a minor modification: medium was replaced 5 and 18 h post-transfection. Cells were harvested and subjected to flow cytometry analysis (FACSaria, Becton Dickinson). The percent of relative expression (%RE) was calculated according to the following: $F=(N_{GFP}\times MI)/N_{LC}$, where F is the fluorescence intensity, N_{GFP} is the number of green fluorescent protein (GFP)-positive cells, MI is the mean GFP intensity and N_{LC} is the total number of live cells; and $\%RE=F_t/F_u$, where F_t is the F of cells transfected with treated plasmids and F_u is the F of cells transfected with undamaged plasmids. Live cells were identified based on altered forward and side scatters. For visualization of GFP and time lapse of GFP repair, a Leica DMi8 fluorescent microscope, equipped with a Leica DFC365FX camera, was used at 10× magnification. Representative videos of *S. carmeli* and rat cells were taken in intervals of 20 min, starting from 24 h post-transfection until 48 h post-transfection.

Statistical analysis

Experiments were repeated three times independently, unless stated otherwise. The data are presented as means±s.d. Two-tailed Student's *t*-tests were used to compare between groups. $P<0.05$ was considered as significant.

RESULTS

Resistance to H_2O_2-induced oxidative stress

It is well established that oxidative stress leads to the accumulation of DNA lesions and to defects in DNA that may promote aging and cancer (Kryston et al., 2011; Barzilai and Yamamoto, 2004; De Bont and Van Larebeke, 2004). We tested the response of *S. carmeli* to oxidative stress induced by H_2O_2, a reactive oxygen species (ROS) that induces both single- and double-strand breaks (SSBs and DSBs, respectively) in DNA. Because ROS levels are elevated under hypoxia and reoxygenation (Chandel et al., 2000), and because *S. carmeli* is a hypoxia-tolerant species, we hypothesized that *S. carmeli* cells would survive H_2O_2 treatment better than the cells of the above-ground rat, and would show lower apoptotic rates in response to the treatment. We estimated the apoptotic cell fraction (subG1 fraction) and the cell cycle distribution of *S. carmeli* and rat primary skin fibroblasts following H_2O_2 treatment (150 µmol l^{-1} for 20 min on ice) by employing flow cytometry of PI-stained nuclei. The results demonstrated a consistent tendency of the rat to have a higher proportion of cells undergoing apoptosis (Fig. 1A,B) compared with *S. carmeli*, with a significant difference at the first time point ($P<0.05$). This is in line with morphological differences of cells in culture, showing higher survival of *S. carmeli* cells following treatment (Fig. 1C). It was also observed that, both in H_2O_2-treated cells and in untreated cells, the ratio between the percentage of cells that are in the G2–M phase to that of cells that are in the S phase is higher in *S. carmeli* compared with the rat (Fig. 1D), with a significant difference under stress conditions at 0–4 h and under control conditions at 24 h ($P<0.05$).

We further tested cell viability rates in *S. carmeli* and rat in response to different concentrations of H_2O_2 (50, 100 and 300 µmol l^{-1} for 30 min on ice) for a period of 4–96 h post-peroxide treatment. In addition, because hypoxia was shown to decrease transcript levels of DNA repair factors in other mammalian species (Klein and Glazer, 2010; Bristow and Hill, 2008), we expected that hypoxia treatment prior to H_2O_2 treatment would deteriorate the effect of H_2O_2 and further reduce cell viability in the rat. In contrast, because *S. carmeli* expresses higher baseline transcripts of DNA repair factors under normoxia than the rat (Malik et al., 2016), a milder or no deterioration was expected for *S. carmeli*. To test this, *S. carmeli* and rat skin fibroblasts were incubated under normoxic or hypoxic conditions (0.5% O_2 for 10 h) and then treated with different concentrations of H_2O_2. Following treatments, cell viability and morphological differences were assessed at several time points. The viability assay confirmed that *S. carmeli* cells are highly resistant to H_2O_2 compared with rat cells (Fig. 1E). This was supported by morphological differences observed under a light microscope (Fig. S2). Additionally, in high doses of H_2O_2, hypoxia pretreatment reduced viability rates in the rat, at most of the time points, compared with normoxic conditions, whereas viability rates in *S. carmeli* remained consistent (Fig. 1F). The experiment was repeated (Fig. S3) and performed under various stress conditions (Fig. S4), showing similar results. To estimate DNA damage following H_2O_2 treatment, we used the alkaline comet assay and γ-H2AX foci quantification to demonstrate the accumulation of DSBs and SSBs, and of only DSBs, following treatment with sub-lethal doses (Fig. S5) of H_2O_2, respectively. These measurements showed that less DNA damage is accumulated in *S. carmeli* compared with the rat (both under control and stress conditions) and that after a comparable recovery period in which all DNA damage is fixed by *S. carmeli* cells (baseline level is reached), rat cells partially recovered their DNA (Fig. 1G,H, Fig. S5).

Resistance to direct genotoxic stress induced by UVC and etoposide

The above experiments demonstrated the resistance of *S. carmeli* to H_2O_2 treatment relative to the rat. Yet, it was still unclear whether this was due to efficient DNA repair and maintenance mechanisms or other reasons, such as cross-species differences in antioxidant defense and H_2O_2 turnover. To address this issue we used two approaches: (1) we performed a functional assay to measure DNA repair capacity; and (2) we challenged *S. carmeli* cells with two additional direct DNA-damaging agents: topoisomerase inhibitor and UV-C radiation. The first stressor, the chemotherapeutic drug etoposide, induces DNA strand breaks by preventing the re-ligation step of topoisomerase type II (Montecucco et al., 2015). Yet, as etoposide could also have species-specific transport/turnover rates, we tested an additional genotoxic stress type, UV-C radiation, for which there are no transport- or turnover-dependent differences between cell lines. For etoposide treatments, medium was replaced with medium containing 50, 100, 150 and 200 µmol l^{-1} etoposide for 24 h, whereas for UV-C treatment, cells were placed in a UV-C crosslinker at doses of 2000, 4000, 6000 and 8000 J m^{-2} UV-C (254 nm wavelength) in the presence of medium. In both treatment types the procedure was repeated in three independent experiments. Similar to oxidative stress resistance, demonstrated above, the

Journal of Experimental Biology (2018) 221, jeb174540. doi:10.1242/jeb.174540

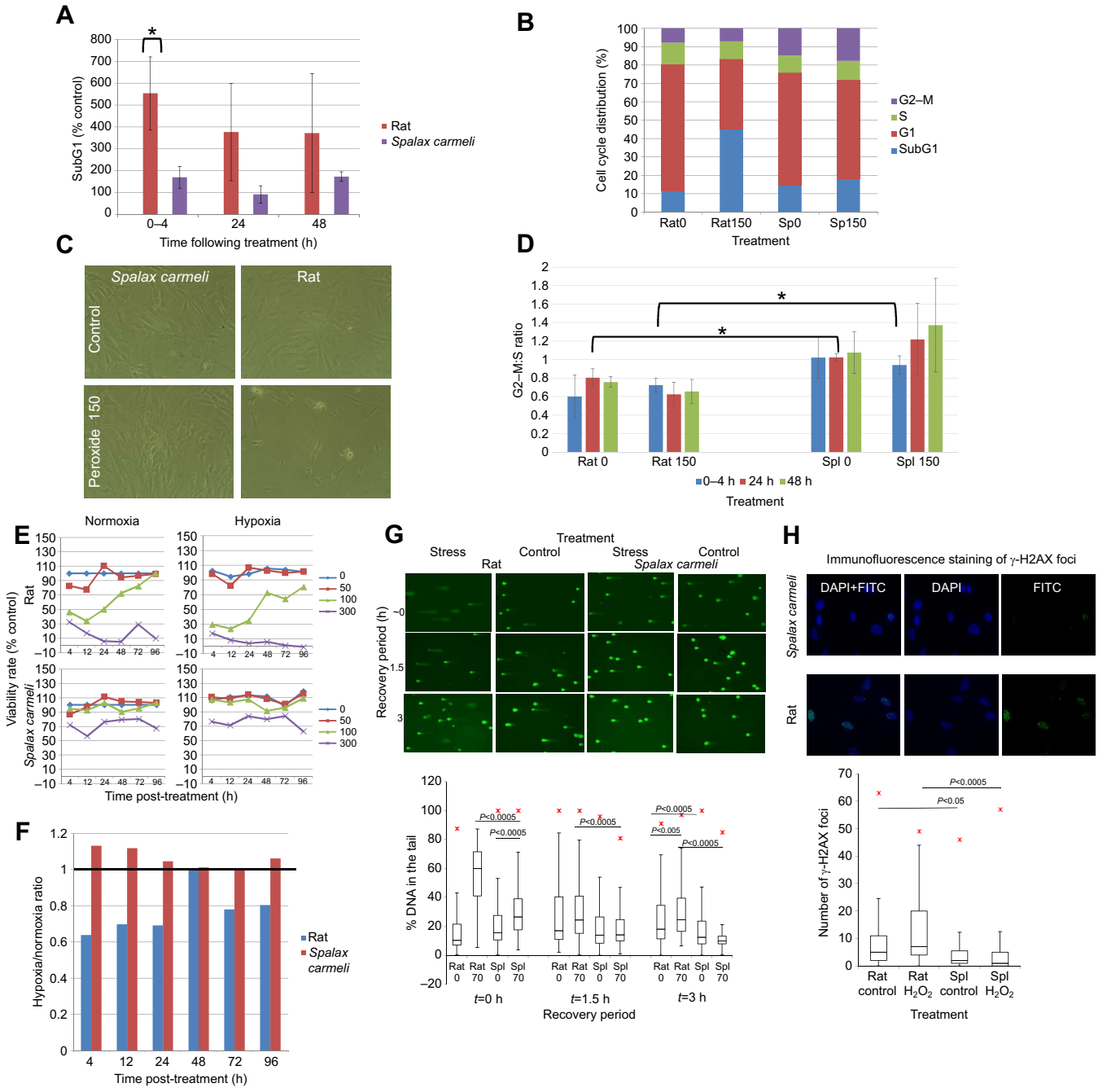

Fig. 1. Response of *Spalax carmeli* and rat (*Rattus norvegicus*) fibroblasts to H_2O_2 treatments. (A) The fraction of apoptotic cells (SubG1) following H_2O_2 treatment presented as percentage of control (untreated cells). Bars represent means±s.d., n=3 independent experiments. P<0.05 for the first time point (two-tailed Student's t-test). (B) Representative cell cycle distribution 48 h following treatment. Representative flow cytometry cell counts are presented in Fig. S1 and Table S2. (C) Representative morphological differences following H_2O_2 treatment. Images were taken 25 h post-treatment. (D) G2–M:S ratio up to 48 h following H_2O_2 treatment in *S. carmeli* and rat. Bars represent means±s.d., n=3 independent experiments. P<0.05 for *S. carmeli* versus rat G2–M:S ratio, under stress at 0–4 h and under control conditions at 24 h (two-tailed Student's t-test). (E) Viability rates of cells treated with H_2O_2 presented as percentage of normoxic control (untreated cells). Absolute values of viability rates are presented in Fig. S6. (F) The ratio between viability rates of cells treated with H_2O_2 following hypoxia and those of cells treated with H_2O_2 without hypoxia pretreatment, as percentage of untreated cells' viability, for *S. carmeli* and rat. This ratio expresses the effect of hypoxia pretreatment on viability rates in response to 100 µmol l^{-1} H_2O_2 treatment. For example, at 24 h *Spalax*'s ratio is close to 1 and therefore almost no differences in response to 100 µmol l^{-1} H_2O_2 were observed between hypoxic and normoxic conditions, whereas the rat's ratio is smaller than 1 (~0.6), indicating that, in this species, hypoxia pretreatment further reduces the viability following 100 µmol l^{-1} H_2O_2. (G) Upper panel: *S. carmeli* and rat skin fibroblasts were treated with 70 µmol l^{-1} H_2O_2 (for 20 min on ice). Cells were thereafter subjected to the comet assay immediately following treatment or following a recovery time of 1.5 or 3 h. Representative images of rat and *S. carmeli* skin fibroblasts' nuclei following electrophoresis under alkaline conditions. Lower panel: box plot diagram of % DNA in the comet tail, representing the amount of DNA damage in the nuclei immediately following 70 µmol l^{-1} H_2O_2 treatment or following a recovery period. Red marks denote maximal outliers. Significant differences between treatments (in the same experiment) are marked by a black line (two-tailed Student's t-test, n>90 nuclei per sample). (H) Upper panel: immunofluorescence and DAPI staining of γ-H2AX foci in rat and *S. carmeli* skin fibroblasts following H_2O_2 treatment. Lower panel: box plot diagram of the number of γ-H2AX foci, representing the number of double-strand breaks formed 60 min following 70 µmol l^{-1} H_2O_2 treatment. Red marks denote maximal outliers. Significant differences between treatments (in the same experiment) are marked by a black line (two-tailed Student's t-test, n>55 nuclei per sample).

Journal of Experimental Biology (2018) 221, jeb174540. doi:10.1242/jeb.174540

results of these experiments showed that *S. carmeli*, relative to the rat, is highly resistant to genotoxic stress induced by etoposide and have a consistent advantage over rat to survive UV-C radiation, with statistically significant differences under specific conditions (Fig. 2; Figs S7–S10). In support, similar to oxidative stress induced by H_2O_2, a lower accumulation of DSBs was observed 1 h following treatment with 50 µmol l^{-1} etoposide for 24 h (Fig. S11), suggesting enhanced mechanisms to prevent and/or repair DNA damage and to maintain genomic integrity in *S. carmeli*.

Enhanced DNA repair capacity of UVC- and H_2O_2-induced lesions

To further test our hypothesis that *S. carmeli* has evolved efficient DNA repair mechanisms, we performed a functional assay that compares DNA repair capacity between *S. carmeli* and rat. We used the flow cytometry-based host cell reactivation assay (F-HCR), which measures the changes in expression of a damaged reporter gene following its repair (Fig. 3A). This assay is not biased by cross-species differences that are not related to DNA repair, as the plasmids' DNA damage is induced outside the cell, in advance, and only then are the plasmids transfected into the cells. In addition, the quantification method of this assay includes normalization of the results according to the non-damaged plasmids (expressed as %RE) (Nagel et al., 2014), which excludes biases related to transfection efficiency and protein expression between the cell lines. The damage to plasmids was introduced by UV-C radiation or H_2O_2 (see Materials and methods), and the test was conducted in four biological repeats. The repair capacity of DNA damage induced by UV-C in *S. carmeli* was ∼5-fold higher than that of the rat in low doses, and 36-fold higher in high doses (two-tailed Student's *t*-test, $P<0.05$; Fig. 3B). In addition, DNA repair capacity of lesions induced by H_2O_2 was ∼5-fold higher in *S. carmeli* compared with the rat (two-tailed Student's *t*-test, $P<0.05$; Fig. 3B). By following GFP expression under a fluorescent microscope (Movies 1 and 2, Fig. 3C lower panel), it was evidenced that the repair of H_2O_2-induced lesions was the earliest among all damage types, all damage types were repaired faster by *S. carmeli* than by the rat, and almost no repair was observed in the high doses of UV-C-treated plasmids in the rat.

DISCUSSION

Genomic instability underlies both cancer and aging, and mutations in genes that are involved in DNA maintenance and repair mediate susceptibility to cancers and progeroid syndromes (Rappaport et al., 2014). *Spalax*'s carcinogen resistance and longevity has been previously studied; nevertheless, none of the studies have directly challenged *Spalax* cells with DNA damage, or tested its DNA repair capacity. It was previously shown that *Spalax*'s unique p53 structure shifts the activation of its target genes by favoring DNA repair and cell cycle arrest over apoptotic gene activation (Shams et al., 2013; Avivi et al., 2007; Ashur-Fabian et al., 2004). This may provide *Spalax* with a greater opportunity to repair DNA damage and other cellular damage before cellular apoptosis is activated, and thus, eventually to reduce the need for the apoptotic response. The present study provides evidences that *S. carmeli* has evolved an enhanced cellular capacity to repair and survive different types of DNA lesions, including those that are induced by UV radiation, which is not present in the subterranean habitat. This suggests a generic mechanism that may allow *S. carmeli* to reduce cellular death events, stress-induced senescence and cellular transformation, providing a better chance of survival in the subterranean habitat, at both the cellular and organismal levels. This may contribute largely to carcinogen resistance, the absence of spontaneous tumorigenesis, resistance to hypoxia–reoxygenation cycles and slow aging in *Spalax*.

It was previously reported that *Spalax* antioxidant activity is improved relative to this of other rodents (Schülke et al., 2012). Here we provided evidence for enhanced efficiency of a second line of defense: DNA repair. We showed that the DNA repair capacity of H_2O_2-induced lesions is five times higher in *S. carmeli* than in the rat.

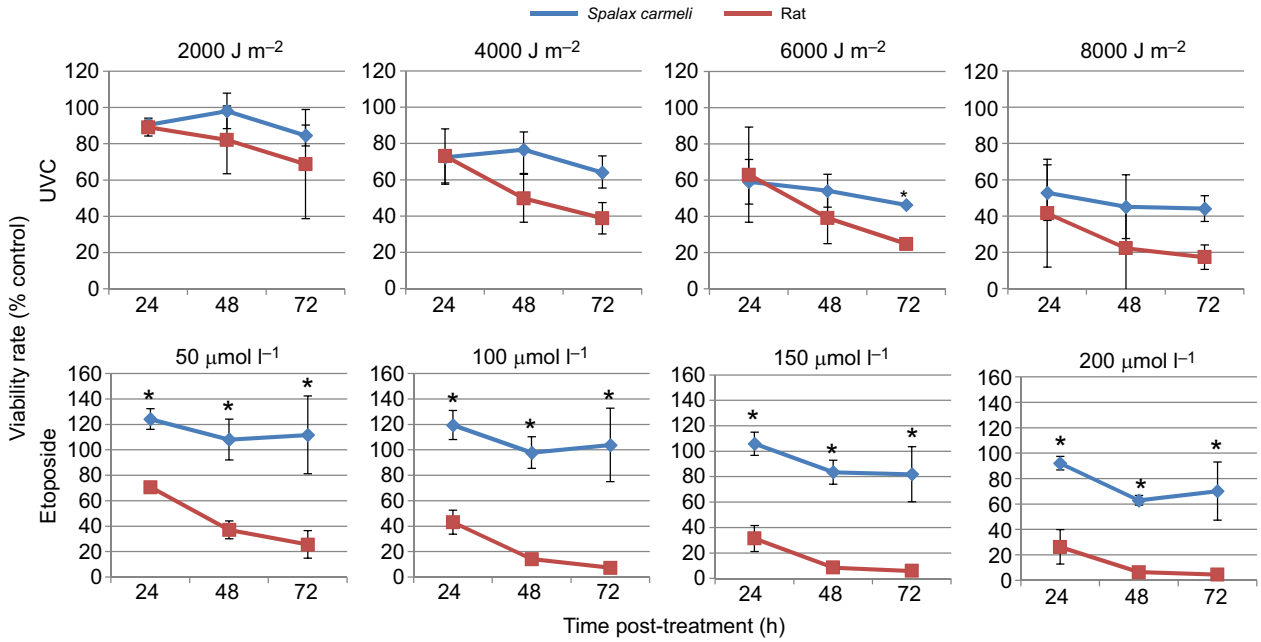

Fig. 2. Viability rates following UV-C and etoposide treatments in *S. carmeli* and rat skin fibroblasts. Upper panel: cells treated with different doses of UV-C radiation (2000, 4000, 6000 and 8000 J m^{-2}). Bars represent means±s.d., $n=3$ independent experiments (two-tailed Student's *t*-test, $P<0.05$ for 6000 J m^{-2} at 72 h). Lower panel: cells treated with different doses of etoposide (50, 100, 150 and 200 µmol l^{-1}) for 24 h. Absolute values of viability rates are presented in Fig. S7. Bars represent means±s.d., $n=3$ independent experiments. $P<0.05$ for all etoposide treatments (two-tailed Student's *t*-test).

Journal of Experimental Biology (2018) 221, jeb174540. doi:10.1242/jeb.174540

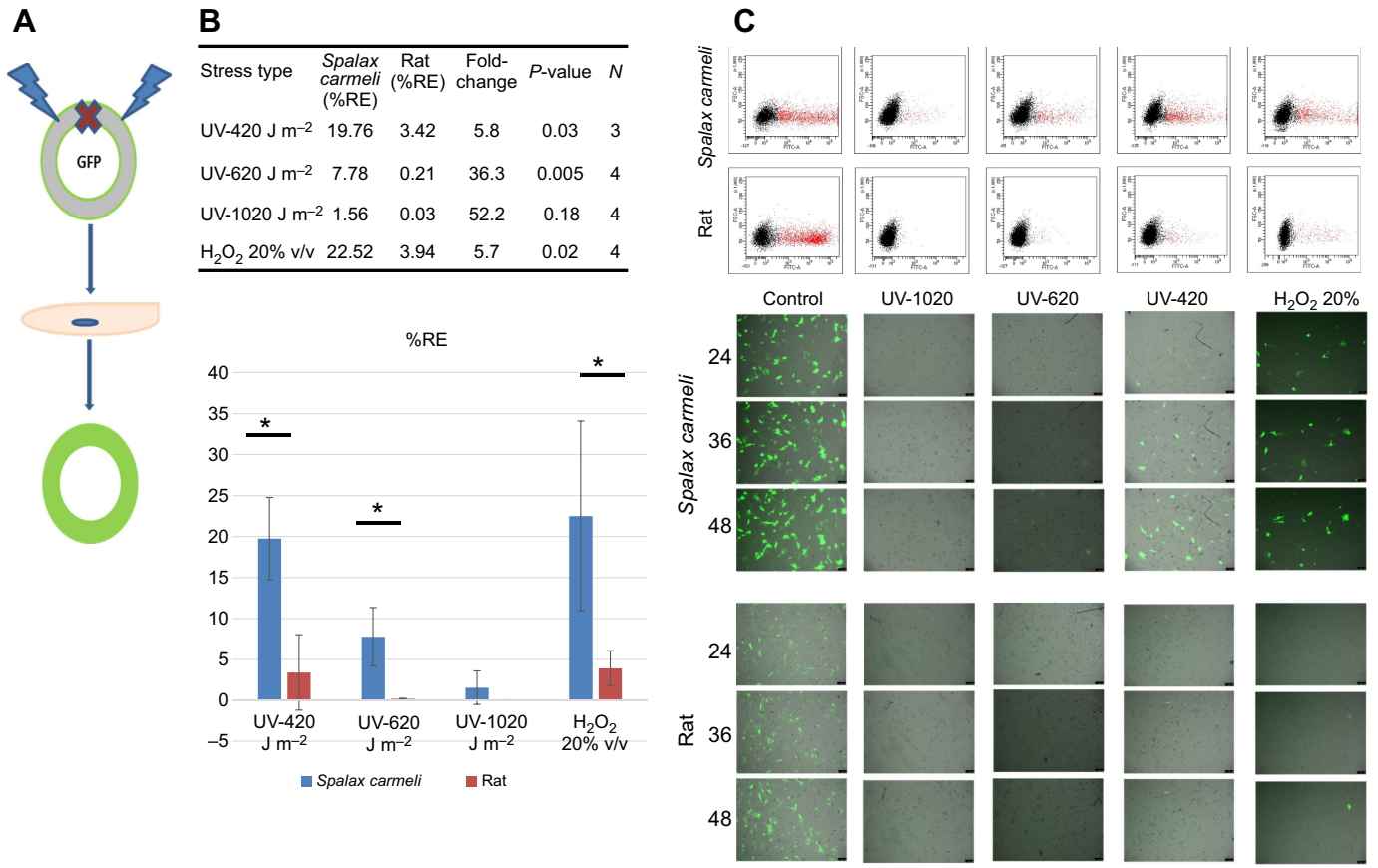

Fig. 3. DNA repair capacity: *S. carmeli* versus rat. (A) Schematic representation of the host cell reactivation assay. *Spalax carmeli* and rat skin fibroblasts were transfected with untreated peGFPN1 plasmids or with peGFPN1 plasmids treated with UV-C/H_2O_2 (damaged plasmid). Following an incubation period of ~53 h post-transfection, cells were harvested and subjected to flow cytometry analysis. The relative expression (%RE, see Materials and methods for formula) of the reporter gene in each cell line was calculated. (B) Upper panel: %RE, fold change, *P*-value and number of biological repeats for each stress type. Lower panel: histogram of *S. carmeli* versus rat %RE (lower panel). Bars represent means±s.d. Significant differences between groups are marked with asterisks (*P<0.05, two-tailed *t*-test). (C) Upper panel: representative images of flow cytometry analysis in *S. carmeli* and rat of a GFP plasmid treated with 0, 420, 620 or 1020 J m^{-2} UV-C radiation or 20% H_2O_2 v/v. Red dots denote GFP-positive cells. Black+red dots denote total live cells. Lower panel: representative fluorescent microscope images of *S. carmeli* and rat skin fibroblast expressing GFP taken 24, 36 and 48 h post-transfection (see also Movies 1 and 2).

Surprisingly, the present study also demonstrated extreme differences in viability rates following etoposide treatment and in repair capacity of UV-C-induced lesions (5- to 36-fold higher), favoring *S. carmeli* over the rat. These results suggest the involvement of the nucleotide excision repair and base excision repair pathways, yet other pathways to repair certain DNA structures such as DSBs and crosslinks pathways may be also involved, for example the homologous recombination and fanconi anemia (FA) pathways (Ramos-Espinosa et al., 2012). The high survival in response to etoposide and the DNA repair capacity of UV-induced DNA damage suggest that *S. carmeli* may have evolved efficient mechanisms to avoid replication stress, as the damage induced by these agents may stall/collapse the replication fork. Namely, the fact that *S. carmeli* resists not only oxidative stress indicates that oxidative DNA damage is not the main or only threat on this species' DNA integrity. The damage induced by other factors (such as reduced dNTPs under hypoxia, for example) may require a repair machinery that is able to cope with high rates of stalled or collapsed forks and DSBs.

In our previous study (Malik et al., 2016), we identified differences in transcript abundance of genes related to recombinational repair, cell cycle regulation (specifically, G2–M checkpoint and kinetochore control) and DNA replication. In the present study (Fig. 1), while the rat cell cycle distribution is in line with the typical mammalian cell cycle phase duration (in which the ratio between the G2−M phases and the S phase is less than 1; Cooper, 2000), the *S. carmeli* cell cycle distribution shows a G2–M:S ratio that is close to or greater than 1. Because no elevations in DNA damage in the *S. carmeli* control groups were observed, these cell cycle characteristics are not likely to be explained by culture conditions, such as atmospheric oxygen sensitivity, which could have slowed down the proliferation rate. Thus, these characteristics may reflect intrinsic strategies to tolerate DNA damage (Livneh et al., 2016), which may have evolved to prevent fork stalling and to expand the DNA repair checkpoint at the G2–M phase. Further investigation, such as S-phase-specific and fork progression studies, is required to answer this research question.

The results presented here emphasize the distinct mechanisms evolved by *S. carmeli* and *H. glaber*. As opposed to our findings presented in the present study, a previous study investigating *H. glaber*'s resistance to several stressors showed that this species is sensitive to H_2O_2 and UV treatments (Salmon et al., 2008). In addition, despite that both species showed differential expression of DNA repair genes, the gene composition may be different between the species. For example, our previous study showed a significant enrichment of DNA replication and FA repair pathways in whole brain tissues that may contribute to the reduction of replication stress in *Spalax* (Malik et al., 2016). The enrichment of the FA pathway was recently identified also in *Spalax*'s liver transcriptome (Schmidt et al., 2017), suggesting a global strategy to overcome

replication stress in these species. To the best of our knowledge, such significant enrichment of the FA pathway was not identified in *H. glaber*, though it was demonstrated that several genes associated with this pathway showed positive correlation with the species' longevity (Ma et al., 2016). We suggest that the requirement to overcome DNA damage in the hypoxic environments may be shared by both subterranean species; however, the 'fine tuning' of the mechanisms evolved in these species are affected by the differences in the lifestyle and atmospheric conditions of their subterranean habitats (Nevo, 2013; Brett, 1991). For example, the sharp fluctuations in O_2 may be milder in *H. glaber*'s burrows owing to soil type and climate conditions. The observed extreme fluctuations in *Spalax*'s burrows may require further protection against replication stress, as the reoxygenation state may result in a greater risk for replication resumption following hypoxia.

The data presented here support the possibility that *Spalax* has evolved mechanisms to cope with the genotoxic threats placed by oxygen fluctuations and hypoxia in the subterranean habitat and that these mechanisms are involved in reducing rates of spontaneous cancers and promoting resistance to carcinogen-induced cancers in this species. In addition, because survival under hypoxic conditions is also a characteristic of tumor cells that do not respond to DNA-damaging treatments (Karakashev and Reginato, 2015), understanding the mechanisms evolved by *Spalax* over millions of years not only has implications for understanding aging and cancer development but also may have therapeutic importance.

Acknowledgements
We thank associate Prof. Irena Manov for her valuable advice on cell culture methods; Dr Olga Raskina for assistance with fluorescent imaging; Dr Sagie Schif for her help with flow cytometry; and Dr Maria Dronin for her advice on immunofluorescence procedures. This work is in partial fulfillment of the requirements for a PhD (V.D.)

Competing interests
The authors declare no competing or financial interests.

Author contributions
Conceptualization: V.D., I.S.; Methodology: V.D., H.E., A.O., I.S.; Software: V.D.; Validation: V.D., I.S.; Formal analysis: V.D.; Investigation: V.D., H.E., A.O., I.S.; Data curation: V.D.; Writing - original draft: V.D., I.S.; Visualization: V.D.; Supervision: I.S.; Project administration: I.S.; Funding acquisition: I.S.

Funding
This study was supported by the John Templeton Foundation (grant 53057) and the Kadas Family (UK).

Supplementary information
Supplementary information available online at
http://jeb.biologists.org/lookup/doi/10.1242/jeb.174540.supplemental

References
Ashur-Fabian, O., Avivi, A., Trakhtenbrot, L., Adamsky, K., Cohen, M., Kajakaro, G., Joel, A., Amariglio, N., Nevo, E. and Rechavi, G. (2004). Evolution of p53 in hypoxia-stressed *Spalax* mimics human tumor mutation. *Proc. Natl. Acad. Sci. USA* **101**, 12236-12241.

Avivi, A., Resnick, M. B., Nevo, E., Joel, A. and Levy, A. P. (1999). Adaptive hypoxic tolerance in the subterranean mole rat *Spalax ehrenbergi*: the role of vascular endothelial growth factor. *FEBS Lett.* **452**, 133-140.

Avivi, A., Ashur-Fabian, O., Joel, A., Trakhtenbrot, L., Adamsky, K., Goldstein, I., Amariglio, N., Rechavi, G. and Nevo, E. (2007). P53 in blind subterranean mole rats–loss-of-function versus gain-of-function activities on newly cloned *Spalax* target genes. *Oncogene* **26**, 2507-2512.

Barzilai, A. and Yamamoto, K.-I. (2004). DNA damage responses to oxidative stress. *DNA Repair* **3**, 1109-1115.

Brett, R. A. (1991). The population structure of naked mole-rat colonies. In *The Biology of the Naked Mole-Rat* (ed. P. W. Sherman, J. U. M. Jarvis and R. D. Alexander), pp. 97-136. Princeton, NJ: Princeton University Press.

Bristow, R. G. and Hill, R. P. (2008). Hypoxia, DNA repair and genetic instability. *Nat. Rev. Cancer* **8**, 180-192.

Buffenstein, R. (2005). The naked mole-rat: a new long-living model for human aging research. *J. Gerontol. Ser. A Biol. Sci. Med. Sci.* **60**, 1369-1377.

Chandel, N. S., Mcclintock, D. S., Feliciano, C. E., Wood, T. M., Melendez, J. A., Rodriguez, A. M. and Schumacker, P. T. (2000). Reactive oxygen species generated at mitochondrial complex III stabilize hypoxia-inducible factor-1alpha during hypoxia: a mechanism of O_2 sensing. *J. Biol. Chem.* **275**, 25130-25138.

Cooper, G. M. (2000). *The Eukaryotic Cell Cycle. The Cell: A Molecular Approach*. 2nd edn. Sunderland, MA: Sinauer Associates.

De Bont, R. and Van Larebeke, N. (2004). Endogenous DNA damage in humans: a review of quantitative data. *Mutagenesis* **19**, 169-185.

Delaney, M. A., Ward, J. M., Walsh, T. F., Chinnadurai, S. K., Kerns, K., Kinsel, M. J. and Treuting, P. M. (2016). Initial case reports of cancer in naked mole-rats (*Heterocephalus glaber*). *Vet. Pathol.* **53**, 691-696.

Domankevich, V., Opatowsky, Y., Malik, A., Korol, A. B., Frenkel, Z., Manov, I., Avivi, A. and Shams, I. (2016). Adaptive patterns in the p53 protein sequence of the hypoxia- and cancer-tolerant blind mole rat *Spalax*. *BMC Evol. Biol.* **16**, 177.

Ellis, M., Stern, O. and Ashur-Fabian, O. (2016). The double benefit of *Spalax* p53: surviving underground hypoxia while defying lung cancer cells in vitro via autophagy and caspase-dependent cell death. *Oncotarget* **7**, 63242-63251.

Fang, X., Seim, I., Huang, Z., Gerashchenko, M. V., Xiong, Z., Turanov, A. A., Zhu, Y., Lobanov, A. V., Fan, D., Yim, S. H. et al. (2014). Adaptations to a subterranean environment and longevity revealed by the analysis of mole rat genomes. *Cell Rep.* **8**, 1354-1364.

Glaysher, S. and Cree, I. A. (2011). Isolation and culture of colon cancer cells and cell lines. *Methods Mol. Biol.* **731**, 135-140.

Gorbunova, V., Hine, C., Tian, X., Ablaeva, J., Gudkov, A. V., Nevo, E. and Seluanov, A. (2012). Cancer resistance in the blind mole rat is mediated by concerted necrotic cell death mechanism. *Proc. Natl. Acad. Sci. USA* **109**, 19392-19396.

Gorbunova, V., Seluanov, A., Zhang, Z., Gladyshev, V. N. and Vijg, J. (2014). Comparative genetics of longevity and cancer: insights from long-lived rodents. *Nat. Rev. Genet.* **15**, 531-540.

Hedges, S. B., Dudley, J. and Kumar, S. (2006). TimeTree: a public knowledge-base of divergence times among organisms. *Bioinformatics* **22**, 2971-2972.

Karakashev, S. V. and Reginato, M. J. (2015). Progress toward overcoming hypoxia-induced resistance to solid tumor therapy. *Cancer Manag. Res.* **7**, 253-264.

Kim, E. B., Fang, X., Fushan, A. A., Huang, Z., Lobanov, A. V., Han, L., Marino, S. M., Sun, X., Turanov, A. A., Yang, P. et al. (2011). Genome sequencing reveals insights into physiology and longevity of the naked mole rat. *Nature* **479**, 223-227.

Klein, T. J. and Glazer, P. M. (2010). The tumor microenvironment and DNA repair. *Semin. Radiat. Oncol.* **20**, 282-287.

Kryston, T. B., Georgiev, A. B., Pissis, P. and Georgakilas, A. G. (2011). Role of oxidative stress and DNA damage in human carcinogenesis. *Mutat. Res.* **711**, 193-201.

Lewis, K. N., Mele, J., Hornsby, P. J. and Buffenstein, R. (2012). Stress resistance in the naked mole-rat: the bare essentials – a mini-review. *Gerontology* **58**, 453-462.

Lewis, K. N., Wason, E., Edrey, Y. H., Kristan, D. M., Nevo, E. and Buffenstein, R. (2015). Regulation of Nrf2 signaling and longevity in naturally long-lived rodents. *Proc. Natl. Acad. Sci. USA* **112**, 3722-3727.

Lewis, K. N., Soifer, I., Melamud, E., Roy, M., Mcisaac, R. S., Hibbs, M. and Buffenstein, R. (2016). Unraveling the message: insights into comparative genomics of the naked mole-rat. *Mamm. Genome* **27**, 259-278.

Livneh, Z., Cohen, I. S., Paz-Elizur, T., Davidovsky, D., Carmi, D., Swain, U. and Mirlas-Neisberg, N. (2016). High-resolution genomic assays provide insight into the division of labor between TLS and HDR in mammalian replication of damaged DNA. *DNA Repair* **44**, 59-67.

Ma, S. and Gladyshev, V. N. (2017). Molecular signatures of longevity: insights from cross-species comparative studies. *Semin. Cell Dev. Biol.* **70**, 190-203.

Ma, S., Upneja, A., Galecki, A., Tsai, Y. M., Burant, C. F., Raskind, S., Zhang, Q., Zhang, Z. D., Seluanov, A., Gorbunova, V. et al. (2016). Cell culture-based profiling across mammals reveals DNA repair and metabolism as determinants of species longevity. *eLife* **5**, e19130.

Macrae, S. L., Croken, M. M. K., Calder, R. B., Aliper, A., Milholland, B., White, R. R., Zhavoronkov, A., Gladyshev, V. N., Seluanov, A., Gorbunova, V. et al. (2015a). DNA repair in species with extreme lifespan differences. *Aging* **7**, 1171-1184.

Macrae, S. L., Zhang, Q., Lemetre, C., Seim, I., Calder, R. B., Hoeijmakers, J., Suh, Y., Gladyshev, V. N., Seluanov, A., Gorbunova, V. et al. (2015b). Comparative analysis of genome maintenance genes in naked mole rat, mouse, and human. *Aging Cell* **14**, 288-291.

Malik, A., Korol, A., Hübner, S., Hernandez, A. G., Thimmapuram, J., Ali, S., Glaser, F., Paz, A., Avivi, A. and Band, M. (2011). Transcriptome sequencing of the blind subterranean mole rat, *Spalax galili*: utility and potential for the discovery of novel evolutionary patterns. *PLoS ONE* **6**, e21227.

Malik, A., Domankevich, V., Lijuan, H., Xiaodong, F., Korol, A., Avivi, A. and Shams, I. (2016). Genome maintenance and bioenergetics of the long-lived hypoxia-tolerant and cancer-resistant blind mole rat, *Spalax*: a cross-species analysis of brain transcriptome. *Sci. Rep.* **6**, 38624.

Manov, I., Hirsh, M., Iancu, T. C., Malik, A., Sotnichenko, N., Band, M., Avivi, A. and Shams, I. (2013). Pronounced cancer resistance in a subterranean rodent, the blind mole-rat, *Spalax*: *in vivo* and *in vitro* evidence. *BMC Biol.* **11**, 91.

Miyawaki, S., Kawamura, Y., Oiwa, Y., Shimizu, A., Hachiya, T., Bono, H., Koya, I., Okada, Y., Kimura, T., Tsuchiya, Y. et al. (2016). Tumour resistance in induced pluripotent stem cells derived from naked mole-rats. *Nat. Commun.* **7**, 11471.

Montecucco, A., Zanetta, F. and Biamonti, G. (2015). Molecular mechanisms of etoposide. *EXCLI J* **14**, 95-108.

Nagel, Z. D., Margulies, C. M., Chaim, I. A., Mcree, S. K., Mazzucato, P., Ahmad, A., Abo, R. P., Butty, V. L., Forget, A. L. and Samson, L. D. (2014). Multiplexed DNA repair assays for multiple lesions and multiple doses via transcription inhibition and transcriptional mutagenesis. *Proc. Natl. Acad. Sci. USA* **111**, E1823-E1832.

Nasser, N. J., Avivi, A., Shafat, I., Edovitsky, E., Zcharia, E., Ilan, N., Vlodavsky, I. and Nevo, E. (2009). Alternatively spliced *Spalax* heparanase inhibits extracellular matrix degradation, tumor growth, and metastasis. *Proc. Natl. Acad. Sci. USA* **106**, 2253-2258.

Nevo, E., Ivanitskaya, E. and Beiles, A. (2001). *Adaptive Radiation of Blind Subterranean Mole Rats.* Leiden, Germany: Backhuys.

Nevo, E. (2013). Stress, adaptation, and speciation in the evolution of the blind mole rat, *Spalax*, in Israel. *Mol. Phylogenet. Evol.* **66**, 515-525.

Pires, I. M., Bencokova, Z., Milani, M., Folkes, L. K., Li, J.-L., Stratford, M. R., Harris, A. L. and Hammond, E. M. (2010). Effects of acute versus chronic hypoxia on DNA damage responses and genomic instability. *Cancer Res.* **70**, 925-935.

Ramos-Espinosa, P., Rojas, E. and Valverde, M. (2012). Differential DNA damage response to UV and hydrogen peroxide depending of differentiation stage in a neuroblastoma model. *Neurotoxicology* **33**, 1086-1095.

Rappaport, N., Twik, M., Nativ, N., Stelzer, G., Bahir, I., Stein, T. I., Safran, M. and Lancet, D. (2014). MalaCards: a comprehensive automatically-mined database of human diseases. *Curr. Protoc. Bioinformatics* **47**, 1.24.1-1.2419.

Salmon, A. B., Sadighi Akha, A. A., Buffenstein, R. and Miller, R. A. (2008). Fibroblasts from naked mole-rats are resistant to multiple forms of cell injury, but sensitive to peroxide, ultraviolet light, and endoplasmic reticulum stress. *J. Gerontol. Ser. A Biol. Sci. Med. Sci.* **63**, 232-241.

Schmidt, H., Malik, A., Bicker, A., Poetzsch, G., Avivi, A., Shams, I. and Hankeln, T. (2017). Hypoxia tolerance, longevity and cancer-resistance in the mole rat *Spalax* – a liver transcriptomics approach. *Sci. Rep.* **7**, 14348.

Schülke, S., Dreidax, D., Malik, A., Burmester, T., Nevo, E., Band, M., Avivi, A. and Hankeln, T. (2012). Living with stress: regulation of antioxidant defense genes in the subterranean, hypoxia-tolerant mole rat, *Spalax*. *Gene* **500**, 199-206.

Shams, I., Avivi, A. and Nevo, E. (2005). Oxygen and carbon dioxide fluctuations in burrows of subterranean blind mole rats indicate tolerance to hypoxic-hypercapnic stresses. *Comp. Biochem. Physiol. A Mol. Integr. Physiol.* **142**, 376-382.

Shams, I., Malik, A., Manov, I., Joel, A., Band, M. and Avivi, A. (2013). Transcription pattern of p53-targeted DNA repair genes in the hypoxia-tolerant subterranean mole rat *Spalax*. *J. Mol. Biol.* **425**, 1111-1118.

Tacutu, R., Craig, T., Budovsky, A., Wuttke, D., Lehmann, G., Taranukha, D., Costa, J., Fraifeld, V. E. and de Magalhães, J. P. (2013). Human ageing genomic resources: integrated databases and tools for the biology and genetics of ageing. *Nucleic Acids Res.* **41**, D1027-D1033.

Tian, X., Azpurua, J., Hine, C., Vaidya, A., Myakishev-Rempel, M., Ablaeva, J., Mao, Z., Nevo, E., Gorbunova, V. and Seluanov, A. (2013). High-molecular-mass hyaluronan mediates the cancer resistance of the naked mole rat. *Nature* **499**, 346-349.

Vinogradov, A. E. (2015). Accelerated pathway evolution in mouse-like rodents involves cell cycle control. *Mamm. Genome* **26**, 609-618.

Zhao, S., Lin, L., Kan, G., Xu, C., Tang, Q., Yu, C., Sun, W., Cai, L., Xu, C. and Cui, S. (2014). High autophagy in the naked mole rat may play a significant role in maintaining good health. *Cell. Physiol. Biochem.* **33**, 321-332.

Table S1 Cell lines of primary skin fibroblasts used in this study

Experiment	**Cells lines**	**Figure**
H_2O_2-hypoxia viability	*Spalax* 2013-A; Rat 2013 -A	Fig. 1
H_2O_2-hypoxia viability	*Spalax* 2013-B; Rat 2015	Fig. S3
H_2O_2-hypoxia viability (diff. settings)	*Spalax* 2013-A ; Rat 2013-A	Fig. S4
H_2O_2-hypoxia viability (diff. settings)	*Spalax* 2013-A ; Rat 2013-A	Fig. S4
Comet assay +pilot for sub lethal dose	*Spalax* 2013-A ; Rat 2013-B	Fig. 1, Fig S5
H_2O_2 staining	*Spalax* 2013-A ; Rat 2013-B	Fig. 1
Etoposide staining	*Spalax* 2013-A ; Rat 2013-B	Fig. S11
Etoposide viability	*Spalax* 2015 ; Rat 2013-B	Fig. 2
Etoposide viability	*Spalax* 2017; Rat 2015	Fig. 2
Etoposide viability	*Spalax* 2017; Rat 2013-B	Fig. 2
UV viability	*Spalax* 2017; Rat 2015	Fig. 2
UV viability	*Spalax* 2013-A; Rat 2013-B	Fig. 2
UV viability	*Spalax* 2017; Rat 2013-B	Fig. 2
Cell cycle	*Spalax* 2013-B ; Rat 2015	Fig. 1
Cell cycle	*Spalax* 2013-B; Rat 2015	Fig. 1
Cell cycle	*Spalax* 2015 ; Rat 2013-B	Fig. 1
HCR	*Spalax* 2013-A ; Rat 2013-B	Fig. 3
HCR	*Spalax* 2017-A; Rat 2015	Fig. 3
HCR	Spalax 2015; Rat 2013-A	Fig. 3
HCR	Spalax 2017-B; Rat 2017	Fig. 3

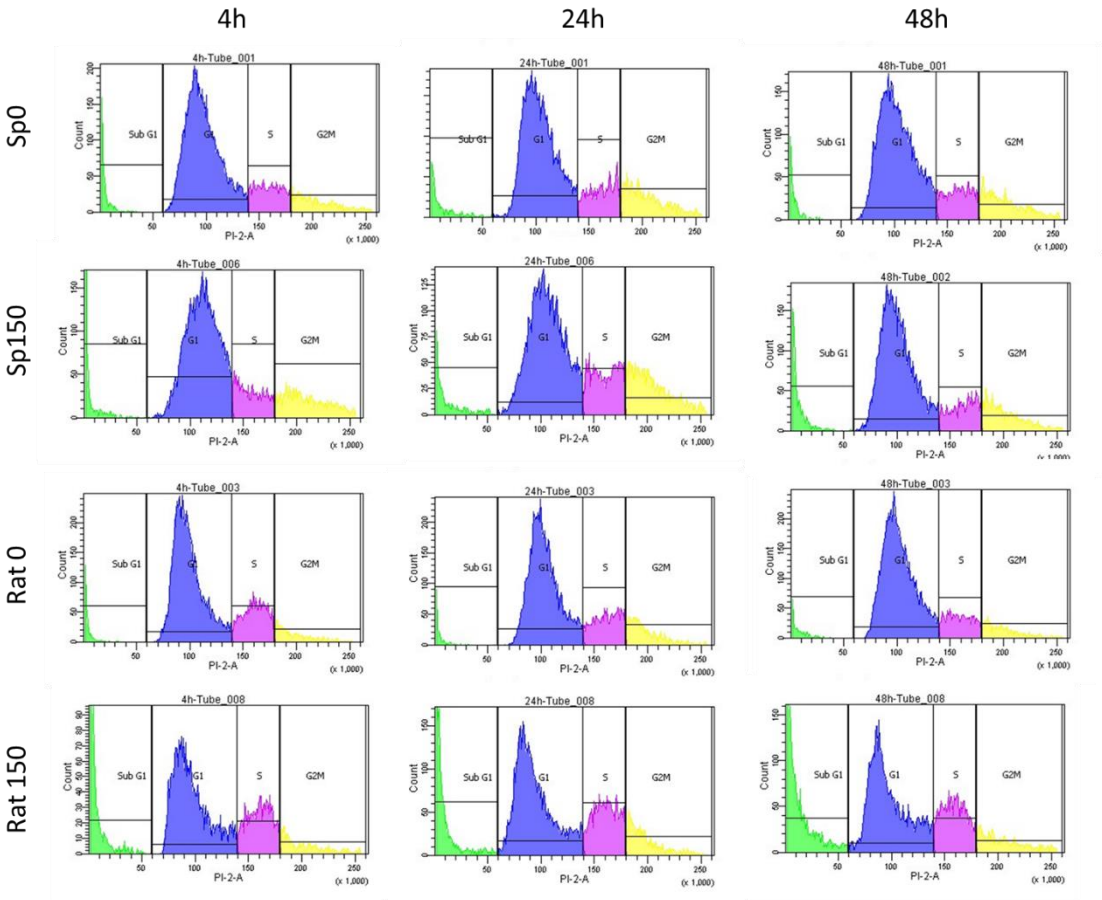

Fig. S1. **Cell Cycle distribution is presented by cell count of PI- stained nuclei.** *Spalax*/ rat cells were treated with 150 μM H_2O_2 and then subjected to cell cycle

distributions assay 4, 24, and 48 hours following treatment. This figure describes one representative experiments out of three (see Fig. 1).

Table S2. C**ell count of cell cycle phases, quantified by flow cytometry of PI- stained nuclei.**

4h	**subg1**	**g1**	**s**
rat0	4.85	62.85	23.95
rat150	22.6	46.3	17.5
sp0	5.25	68.6	12.05
sp150	6.5	68.45	12.45
24h	**subg1**	**g1**	**s**
rat0	3.1	64.75	18.5
rat150	15.9	50.25	22.5
sp0	4.8	59.55	17.95
sp150	6.5	57.6	18.1
48h	**subg1**	**g1**	**s**
rat0	3.25	71.35	14.35
rat150	21.95	47.85	19.85
sp0	5.75	67.75	14.1
sp150	8.5	63.75	15.65

Spalax/ rat cells were treated with 150 µM H_2O_2 and then subjected to cell cycle distributions assay 4, 24, and 48 hours following treatment. The values represent the

average of two duplicates in a single experiment, measuring the fraction of cells in each cell cycle phase.

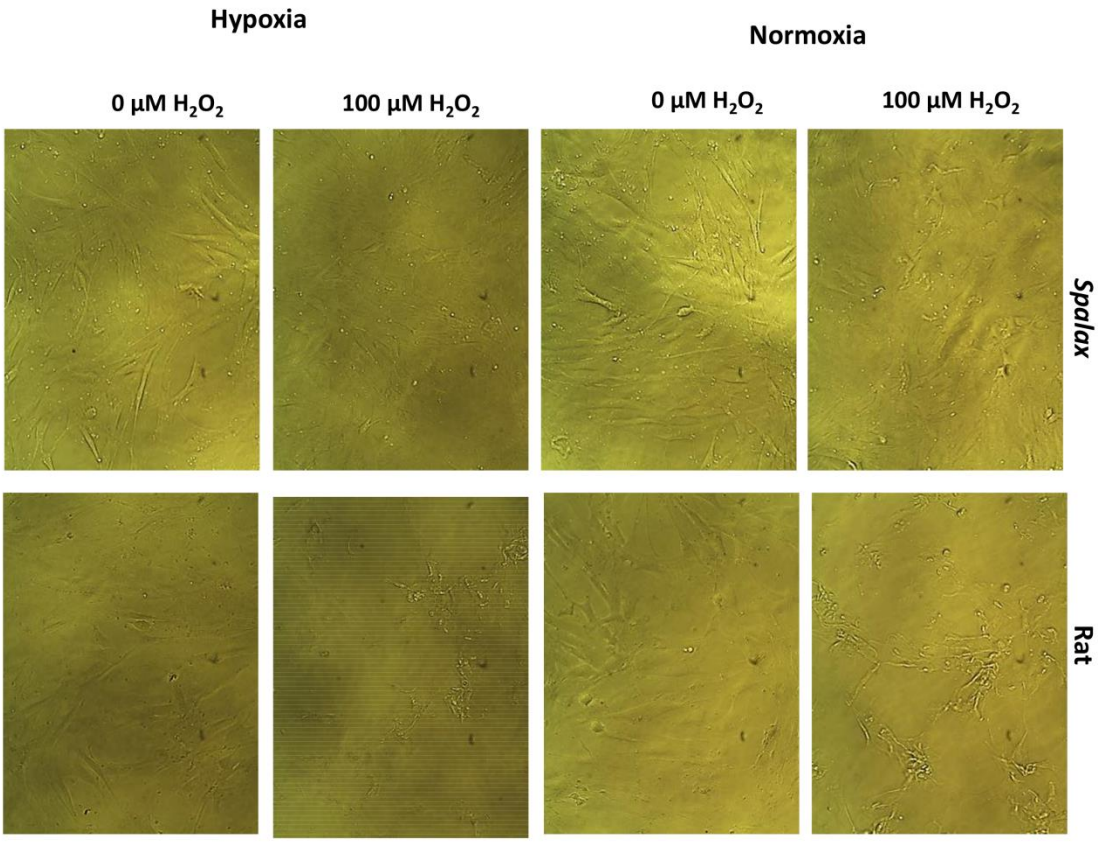

Fig. S2.*Spalax*/rat skin fibroblasts morphology following treatment with 100 µM H_2O_2 (with or without hypoxia pre-treatment). Images were taken 27 hours post hypoxia.

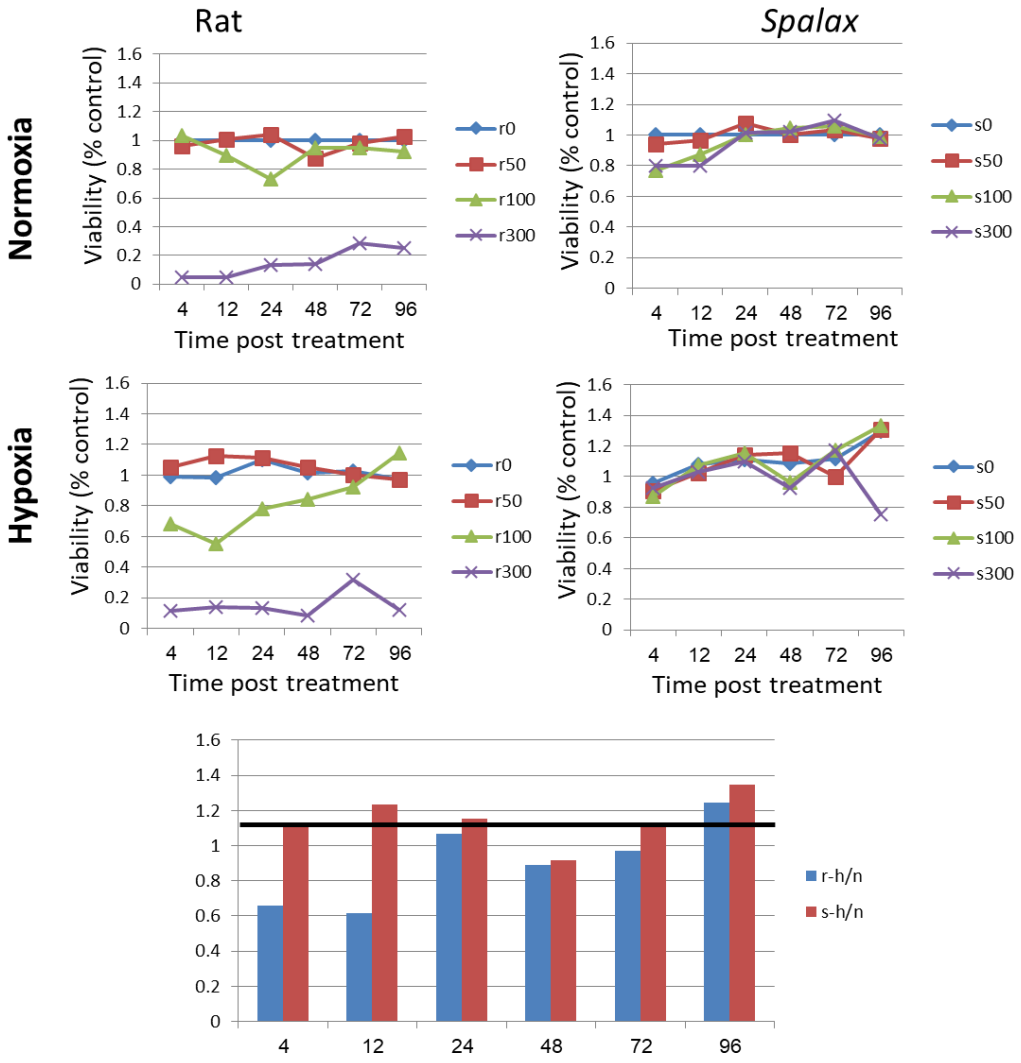

Fig. S3. **Viability of cells following peroxide treatment**: Biological repeat of the experiment presented in Fig. 1. Rat ("r) and *Spalax* ("s") skin fibroblasts' cell lines were isolated from different rat and *Spalax* individuals (see Table S1). Cells were then either incubated in hypoxic or in normoxic conditions and treated with different concentrations of peroxide. Viability rates were measured in different incubation periods post treatments.

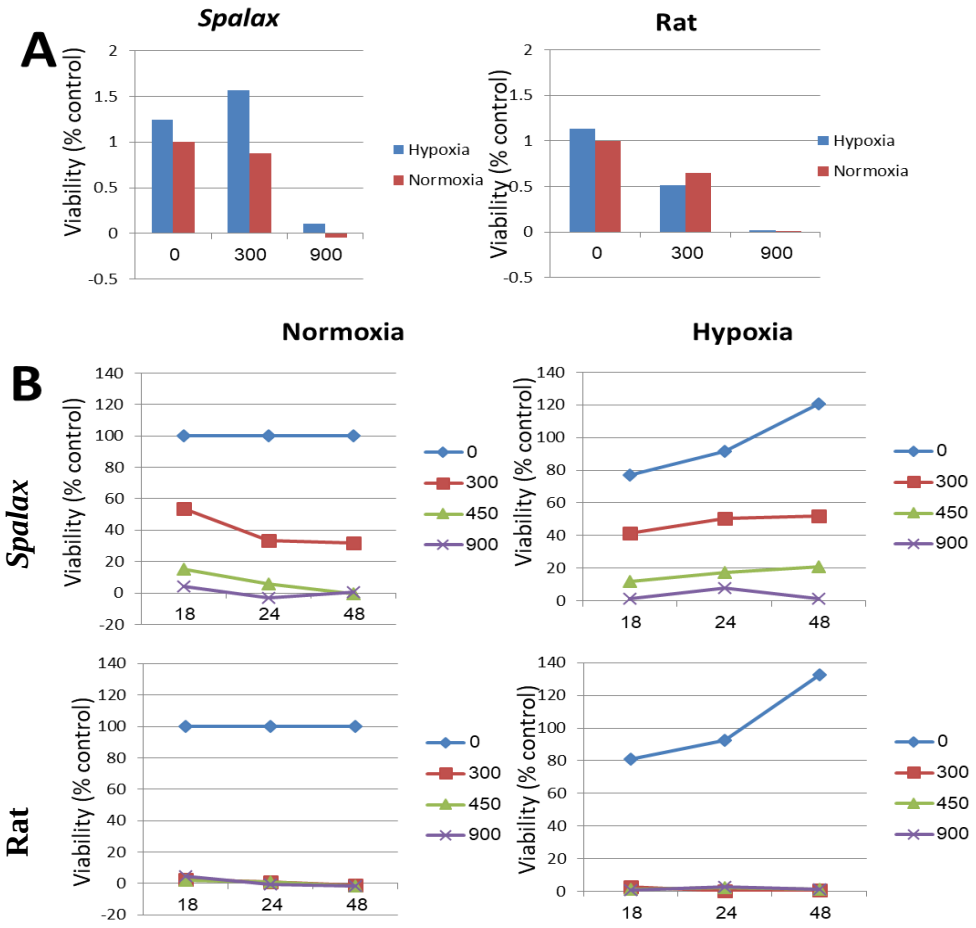

Fig. S4. Viability rates of *Spalax* and rat skin fibroblasts are presented as percentages from normoxic control. Cells were either incubated under hypoxic or normoxic conditions and then treated with H_2O_2 (see Table S3 for specific experimental settings).

Table S3. Experimental settings for testing resistance to oxidative stress in combination with hypoxia in *Spalax* and rat skin fibroblasts

Modified settings	**Fig. 2**	**Fig. S4**
H_2O_2 incubation conditions	30 minutes, on ice	1 hour, room temperature
H_2O_2 doses	300 µM H_2O_2 and below	300 µM H_2O_2 and above
Hypoxia duration	10 hours	4 hours
O_2 percent	0.5%	1%
Time point	4-96 hours post H_2O_2 treatment	**Fig. S4A** - 3 hours post H_2O_2 treatment **Fig S4B**- 18-48 hours post H_2O_2 treatment

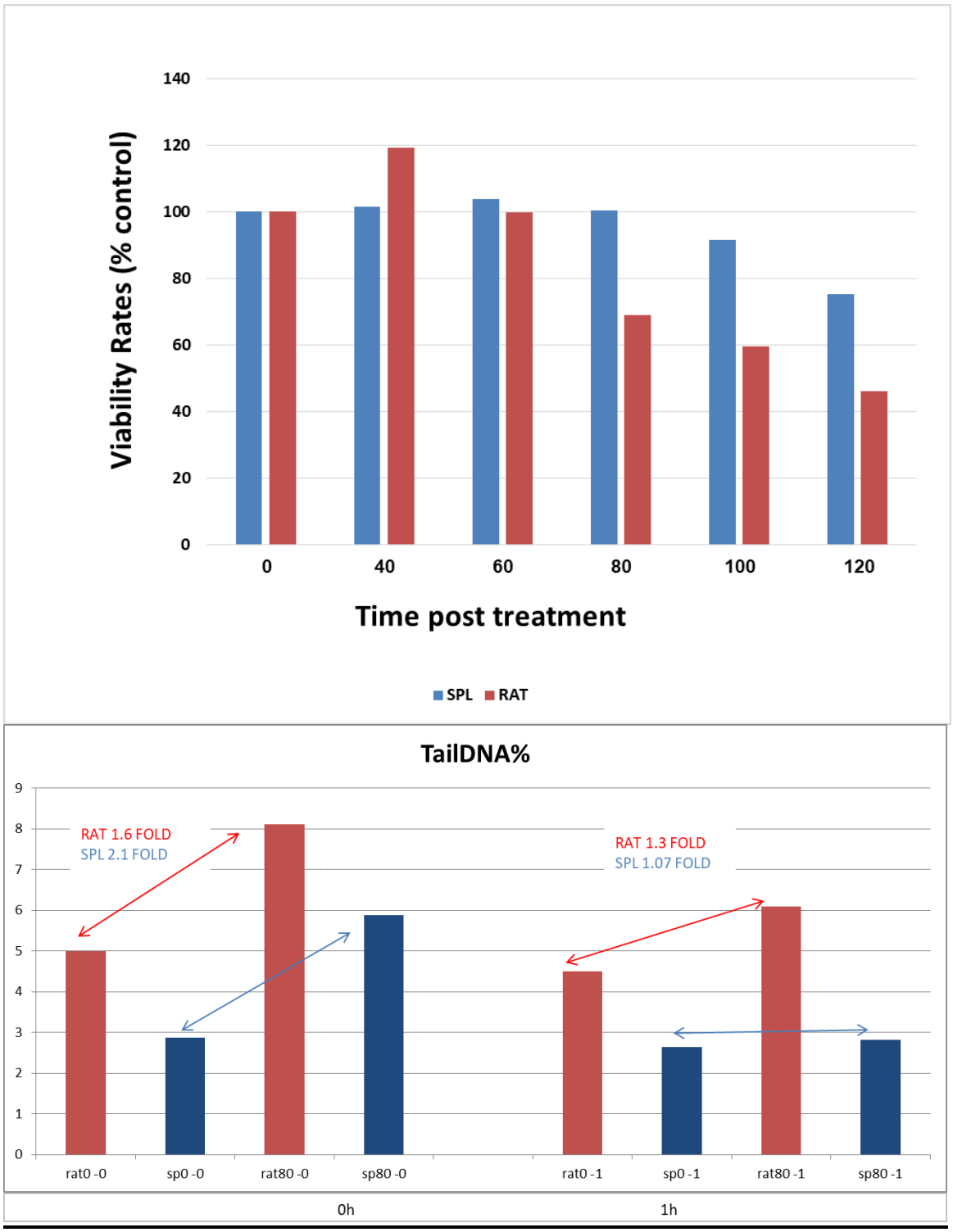

Fig. S5. Upper panel- Viability assay used as a pilot experiment to determine the sub-lethal peroxide dose in *Spalax* and rat skin fibroblast to be thereafter used for the comet assay. **Lower panel-** Additional Comet assay experiment. Cells where treated with 80µM H_2O_2 for 20 minutes on ice and then recovered for 0/1 hours. Cells where thereafter subjected to the comet assay. Median values of % DNA in the tail are presented.

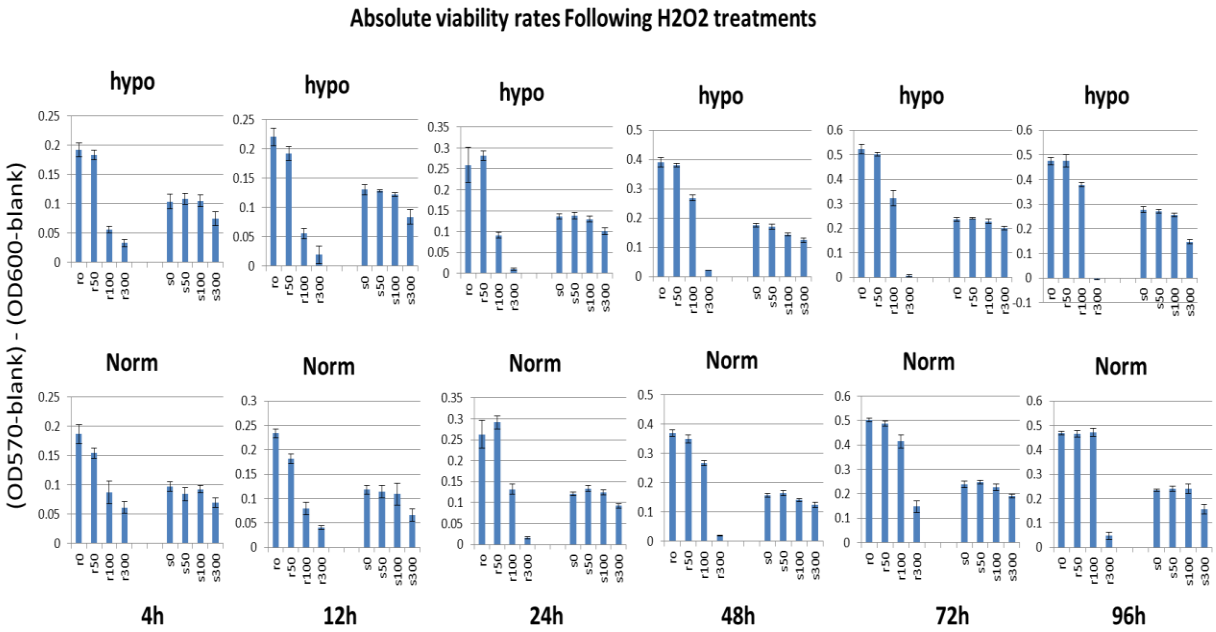

Fig. S6 Absolute viability rates of *Spalax* ("s") vs. rat ("r") cells treated with peroxide following hypoxia/normoxia. Cells where either treated with hypoxia or incubated in ambient air. Then cells where treated with different doses of peroxide (50, 100, 300 µM). PrestoBlue© reagent was used to asses cells' viability 4-96 hours post

treatments. This figure describes one representative experiments out of two (see Fig. 1). Error bars denotes SD of technical replicates.

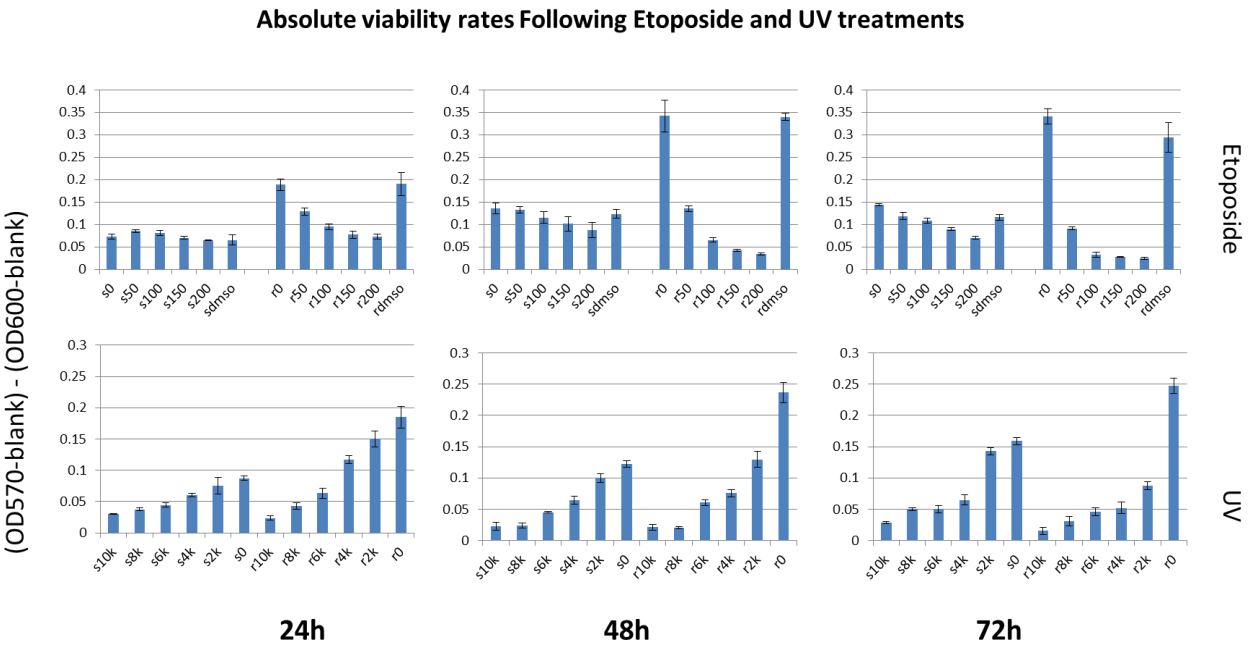

Fig. S7. Absolute viability rates of *Spalax* ("s") vs. rat ("r") cells treated with etoposide and UVC. Cells where treated with etoposide and UVC in different doses. PrestoBlue© reagent was used to asses cells' viability 24-72 hours post treatments. This

figure describes one representative experiments out of three (see Fig. 3). Error bars denotes SD of technical replicates.

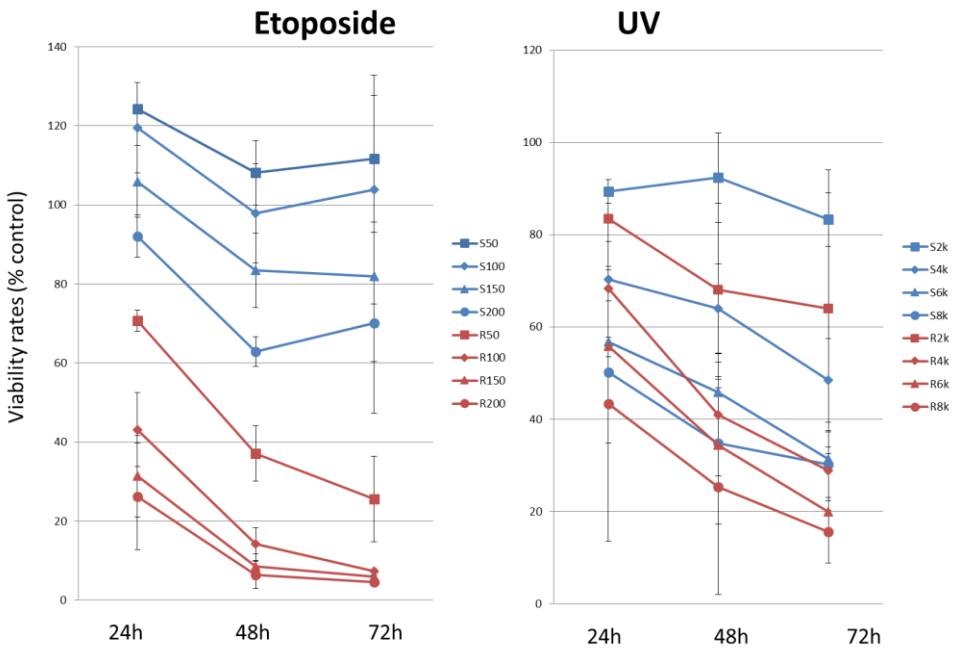

Fig. S8. Viability rates (%control) following UV and etoposide treatments in *Spalax* ("S") and rat ("R") cells, which are presented in several panels in Fig. 2, are presented here in the same graph.

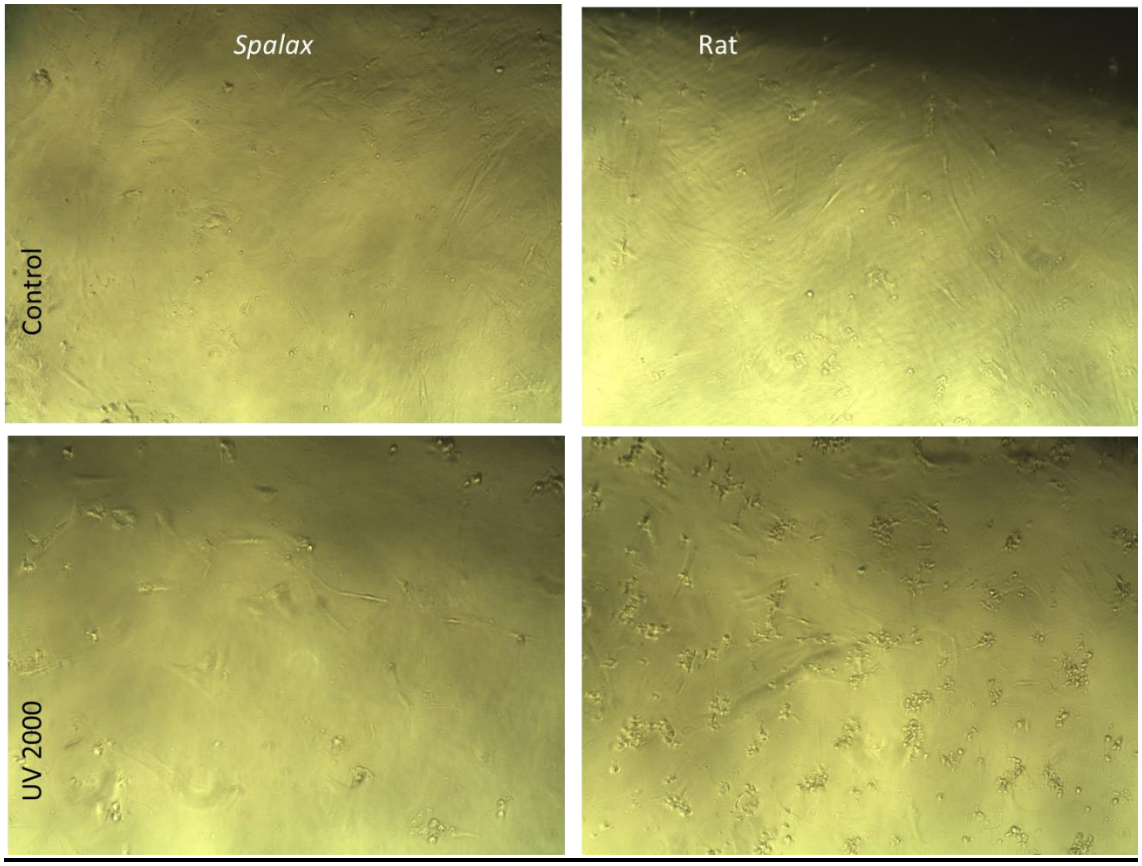

Fig. S9 Morphology of rat and *Spalax* skin fibroblasts that were treated with 2000 J/m^2 UVC. Images were taken 54 hours post treatment

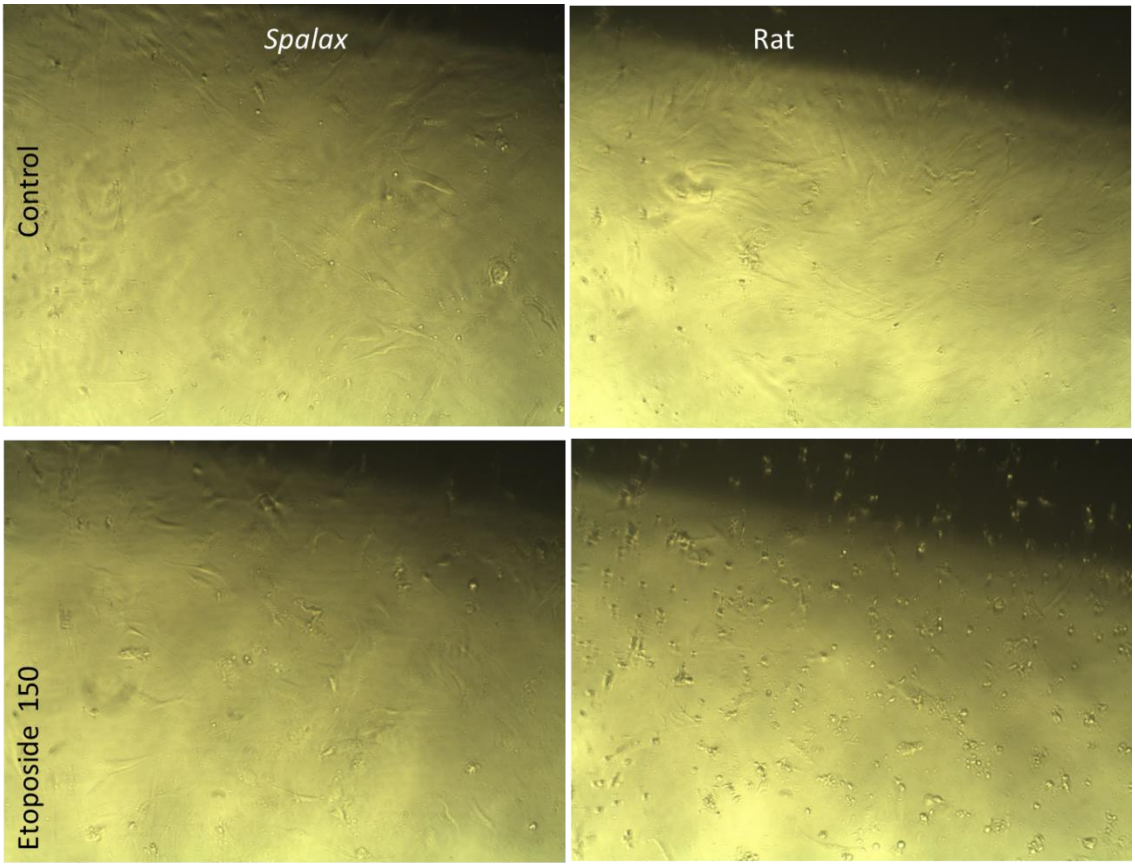

Fig. S10 Morphology of rat and *Spalax* skin fibroblasts that were treated with 150 µM etoposide. Images were taken 30 hours post treatment

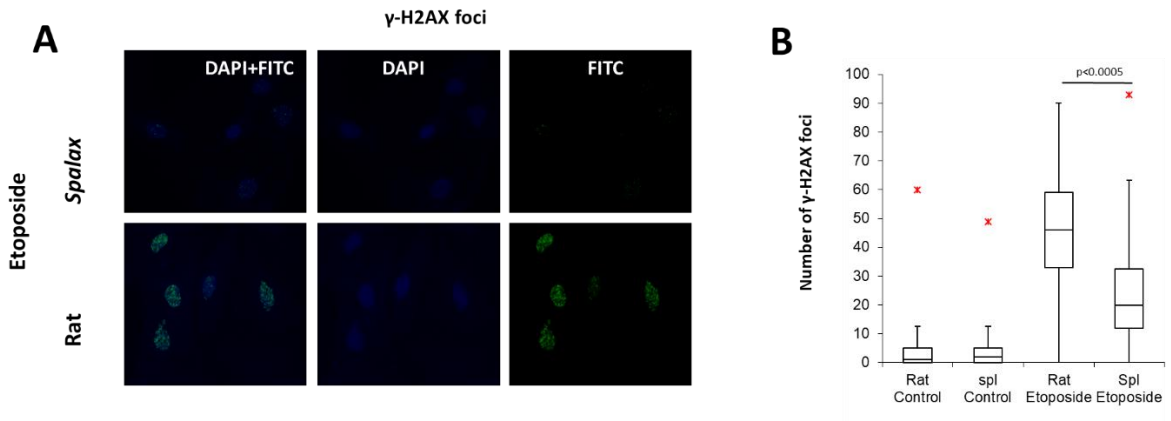

Fig. S11. Immunofluorescent staining of γ-H2AX foci in rat and *Spalax* skin fibroblasts following etoposide treatment of 50 µM, for 24 hours. Cells were fixated 60 minutes after treatment. **A.** Representative images of rat and *Spalax* skin fibroblasts' nuclei γ-H2AX foci and DAPI stating are presented. **B.** The number of γ-H2AX foci, quantified by FociCounter software, represents the number of DSBs formed 60 minutes following 50µM etoposide treatment. At least 55 nuclei were analyzed for γ-H2AX foci is each sample.

Movie 1

Spalax skin fibroblasts 24-48 hours following transfection with GFP plasmid that was treated with 420 J/m^2 UVC radiation. The overlay between FICT and DIC channels is presented in Fig. 3 for 24, 36, and 48 hours post transfection.

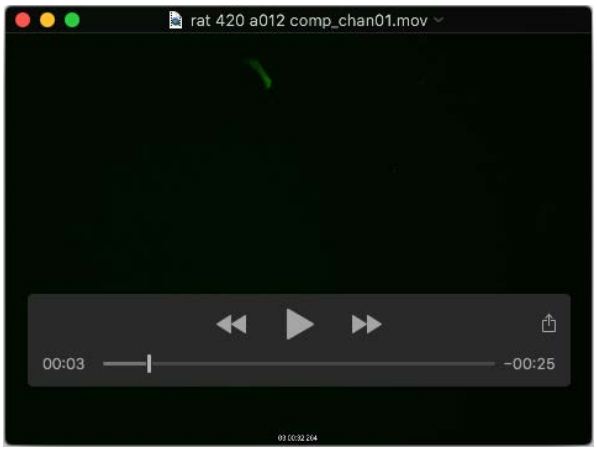

Movie 2

Rat skin fibroblasts 24-48 hours following transfection with GFP plasmid that was treated with 420 J/m2 UVC radiation. The overlay between FICT and DIC channels is presented in Fig. 3 for 24, 36, and 48 hours post transfection.